Mineral-PET : Kimberlite sorting by nuclear-medical technology

S. Ballestrero[a], F. Bornman[b], L. Cafferty[b], R. Caveney[c], S.H. Connell[a], M. Cook[a], M. Dalton[d], H. Gopal[b], N. Ives[c], C.A. Lee[a], W. Mampe[e], M. Phoku[e], A. Roodt[b], W. Sibande[a], J.P.F. Sellschop[c,g], J. Topkin[f], D.A. Unwuchola[a].*

a - University of Johannesburg, Johannesburg, South Africa.
b - Bateman Engineering, Boksburg, South Africa.
c - University of Witwatersrand, Johannesburg, South Africa.
d - University of Virginia - Virginia, USA.
e - North West University - Mafikeng, Mmabatho, South Africa.
f - Nuclear Energy Corporation of South Africa (NECSA).
g - In Memoriam, deceased.

Abstract

A revolutionary new technology for diamond bearing rock sorting which has its roots in medical-nuclear physics has been taken through a substantial part of the R&D phase. This has led to the construction of the technology demonstrator. Experiments using the technology demonstrator and experiments at a hospital have established the scientific and technological viability of the project.

1 Introduction

The extraction of diamonds from the excavated rocks is presently a complex process which requires large amounts of equipment, energy and water. The large rocks are initially reduced in size, by means of a crusher (for example with counter-rotating cylinders) to particles of approximately 10 - 15 cm, using water both to cool the system and to contain volatile dust. This "first crush" is then further crushed, in one or two passes, down to a size of few millimetres. It is then assumed that in this final "final crush" the diamonds are going to be exposed at the surface, and one of two techniques are used: dense media separation and either the traditional grease table, or X-ray absorption [1]. Only a minute fraction of the first crush actually contains any significant diamond particles, and in practice most of the energy, water and machinery are wasted on processing barren material. It is the realization of this glaring inefficiency that prompted research on the topic of early rejection of barren kimberlite rocks. An optimally efficient sorting technology operating on the coarse crushed material would then save up to 98% of the energy and water, substantially reduce the size and cost of the downstream processing machinery, as well as reducing the chance that larger diamonds are damaged.

The envisaged method, named Mineral-PET, is a kimberlite ore sorting technology [2]. It deploys the model based, statistical, quantitative analysis of the spatial localization of sources of positron emissions to recognize the presence of diamond within kimberlite. The method is to be applied in an online context at the diamond mine itself. The "PET" acronym is derived from Positron Emission Tomography, the well know application of nuclear imaging techniques in diagnostic medicine [3]. As positron emission by natural carbon does not occur spontaneously, it is necessary to produce the positron emitting ^{11}C PET isotope by a suitable transmutation reaction on natural ^{12}C. This can be accomplished by photonuclear reactions, namely the ^{12}C(γ,n)^{11}C reaction, which presents the largest cross section ($\sim$8 millibarn) for impinging photons of around 23 MeV corresponding to the centre of the Giant Dipole Resonance (GDR). Such photons can be efficiently generated by bremsstrahlung of electrons on high-Z materials. This activation stage of the Mineral-PET process is to be carried out on kimberlite feed rock which has been course crushed to a diameter of about 10 cm. This is equivalent to the first crush stage of the current process described above. The amount of positron emission signatures from the activated ^{11}C in the

*sergio.ballestrero@cern.ch

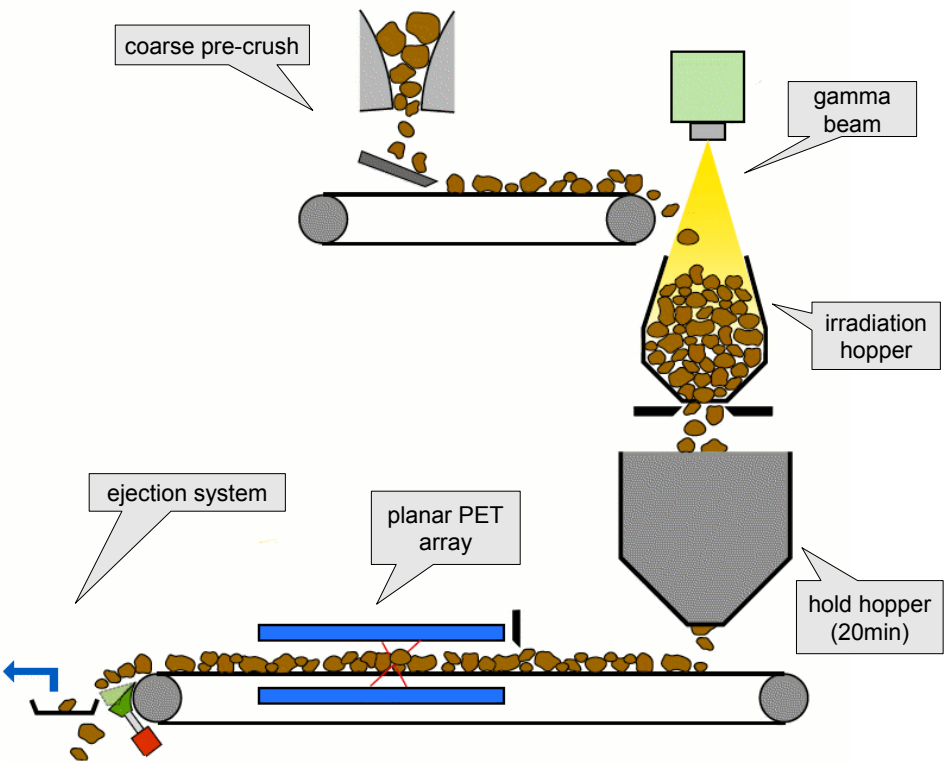

Fig. 1: The Mineral-PET concept: One deploys a planar PET array to detect the PET image from activated diamond bearing kimberlite rock in real time on a conveyor belt in an online mining situation.

diamonds is very high compared to the surrounding material, but insufficient for diamond identification against the background of the integral emissions from the activated ^{11}C derived from dilute non-diamond carbon in the much larger host volume (see section 2.2).

It is therefore necessary to go beyond simple counting techniques, and to partially image the positron emitter density inside the sample. The assumption here is that carbon in diamond form is spatially localized, whereas non-diamond carbon (present in certain minerals within the kimberlite breccia) is homogeneously distributed. One also expects to simultaneously activate the oxygen PET isotope, ^{15}O, which is present to the level of about 50% in the kimberlite breccia. Fortunately, this is a time dependent background, as the lifetime of ^{15}O is about 10 times shorter than that of ^{11}C. It is therefore necessary to allow time for the ^{15}O PET activity to decay before attempting to image the ^{11}C PET activity. This is done in a hold hopper. Finally, sufficient imaging information for discriminating diamond-bearing rocks from barren rocks must be acquired in the shortest possible time, to allow for processing of large amounts of material. This requires both detection and quasi-image reconstruction techniques which are substantial developments over those used in nuclear medicine.

The process of coarse pre-crush, PET isotope activation, hold hopper and diamondiferous kimberlite rock particle detection by the linear PET array are indicated in Fig. 1. Diamond containing rocks are removed by an ejection system triggered by a signal from the planar PET array. In the discussion below, we will consider a specific design scenario where the conveyor belt delivery system for run-of-mine conditions are up to 1000 tons per hour with a belt speed of 2 m/s. The activation and detection times for a given rock particle are 1 s each. Mineral-PET is extremely demanding in that it must be performed in real time under mining conditions, while Medical-PET is implemented under essentially laboratory conditions and the data acquisition times are minutes or much longer.

The development of the initial concept into a process which is viable at an industrial scale requires

further understanding of the physics involved both in the activation and in the detection processes, and the development of new imaging techniques, building on concepts from other disciplines. One important tool has been the detailed and accurate Monte Carlo models and simulations for each component and for the complete process. These models were validated using experiments based on a small scale technology demonstrator. The technology demonstrator made use of kimberlite "phantoms" which passed through a planar PET system on a conveyor belt. The phantoms consisted of reconstituted kimberlite powder which had been homogeneously premixed with the positron emitter ^{22}Na. The reconstitution process used technology for radiation waste permanent storage, considering the background activity of the phantom. Diamonds were modeled in the phantom by the inclusion of a localized "hot-spot" of ^{22}Na. The activities of the homogeneous background as well as the localized PET emissions correlated with what was expected from kimberlite rock which had been subjected to the photon irradiation mentioned above. This procedure was used to investigate the scientific feasibility of the Mineral-PET concept.

2 Activation

This section includes all the considerations which lead to the production of sufficient ^{11}C PET activity in the kimberlite rock stream. It also considers implications of the associated non-PET activation of the kimberlite and the diamond.

2.1 The (γ,n) Nuclear Reaction

In order to create a positron emitting isotope from natural carbon, ^{12}C, the most favourable process has been identified to be the ^{12}C$(\gamma, n)^{11}$C photonuclear interaction in the GDR resonance regime. Compared to other ^{12}C(*,*)^{11}C processes that could be considered, it seems to offer a better balance of high cross section, selectivity, and low production of undesired secondaries. In particular the (e^-, n) interaction, a most interesting candidate because it would make direct use of the charged particle beam, has a cross section which is much lower in first approximation by a factor $1/137$, because it proceeds through the emission of a virtual photon by the e^-, resulting in a lower compound efficiency. The photonuclear interactions in the GDR regime operate mostly via the creation of a metastable excited nucleus, followed by its thermalization and decay to a stable daughter via the "evaporation" of one or more nucleons, possibly followed by a gamma cascade. Following the discovery of the GDR [4], Goldhaber and Teller introduced an elementary model of the interaction phase based on the relative oscillation of the proton and neutron components [5]; with minimal refinements [6], this model is able to predict the basic behaviour. More advanced models (nuclear hydrodynamics and refinements [7, 8]) are able to produce accurate predictions for medium to heavy nuclei. For the light nuclei of interest in this research the collective models are not appropriate [9], and it is necessary to consider microscopic models (usually particle-hole excitation states on a shell model basis) and the non-negligible contribution of the direct $\gamma + n \rightarrow n$ interaction [10]; these sophisticated models are useful for the interpretation, but not yet able to produce accurate predictions [11, 12]. For the later de-excitation phase, instead, the pre-equilibrium evaporation models produce sufficiently accurate results [13, 14]. Figures 2–3 display the GDR cross sections for the ^{12}C(γ, xn) and ^{16}O(γ, xn) reactions.

2.2 Sources of background

The broad spectrum of bremsstrahlung photons also interacts with the material surrounding the diamond - most usually kimberlite. Kimberlites are a class of deep-earth composite rocks; while their petrographic composition does vary considerably, the average chemical composition is relatively stable. With this knowledge it is possible to study the effects of the γ irradiation to address both radiation protection requirements, and possible concerns on permanent damage or long term activity of the diamonds and of the tailings. Many different radioisotopes may possibly be generated, either directly via the same (γ, n) reaction and other primary $(\gamma, *)$ reactions, but also secondary $(n, *)$, $(p, *)$ reactions need consideration.

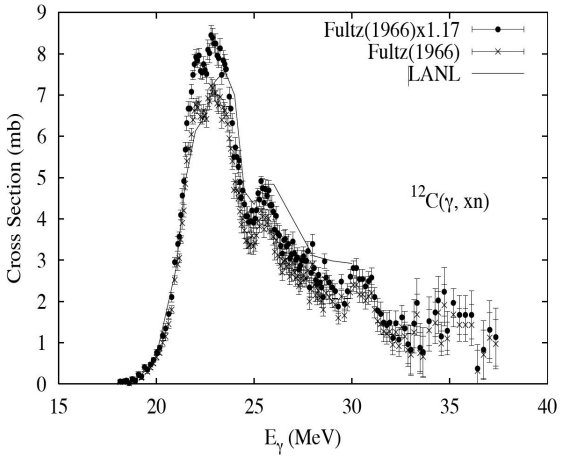

Fig. 2: Cross sections for the ^{12}C(γ, xn) reaction at the dipole resonance [13].

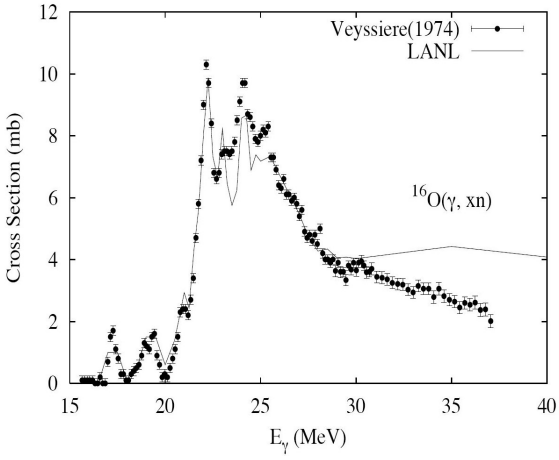

Fig. 3: Cross sections for the ^{16}O(γ, xn) reaction at the dipole resonance [13].

In addition, for the most abundantly generated isotopes, the possibility of photonuclear reactions must also be considered, because of the time span of the irradiation.

Besides the carbon - which is present both concentrated in diamonds and as a trace element in the host rock - of particular interest is oxygen, which is present in large amounts (in the form of silicon oxide and other oxides, and water), constituting approximately 48% of the rock mass. The ^{16}O$(\gamma, n)^{15}$O photo-production reaction has a very similar cross section to that of the ^{12}C$(\gamma, n)^{11}$C photo-production reaction (Figures 2–3). It is therefore not possible to avoid the production of the radioactive ^{15}O isotope by choosing a different irradiation energy range; this is most relevant because ^{15}O is a positron emitter just like ^{11}C, so that these events cannot be differentiated by the detectors. But there are still two characteristics that differentiate oxygen from carbon in this setting: firstly, oxygen is homogeneously distributed in the kimberlite, while carbon is concentrated almost exclusively in the diamonds; secondly, ^{15}O has a much shorter half-life, of approximately 2 minutes, compared to ^{11}C with its 20 minutes half life. Allowing sufficient time before the detection, the positron emission activity from ^{15}O can be reduced to a level that it is similar to or less than that of homogeneously distributed non-diamond carbon in the kimberlite. The diamond identification can then proceed by detecting a statistically significant localization of PET emitters in a homogeneous background of PET emitters.

To asses the background in the Mineral-PET technique and to study the long term activation in materials relevant to Mineral-PET, irradiation studies were performed. The irradiated materials were kimberlites, country rock and diamond (specifically Kimberlite, Kimberlite Breccia, Hypabissal Kimberlite, Amphibolite, Dolomite, Biotite gneiss, Quartz feldspar gneiss, Biotite Schist, Quartzite, Kimberlite spiked with diamond and 9 diamonds of mixed types, with different inclusions). The irradiation experiments were carried out using a bremsstrahlung photon beam produced by a 40 MeV electron beam on 3 mm of tungsten to a dose of 50 Grays. These irradiations were performed at the Scanditronix RTM 50 Racetrack Microtron at the Karolinska Institutet in Sweden. The irradiation products were studied with a gamma spectrometer which could operate in singles mode with a HPGe detector (arbitrary decay photon identification) and in coincidence mode with a NaI detector (so that the PET emissions could be separately identified). The data acquisition was also taken in a time differential event-by-event mode. This enabled flexible off line time histogramming of the different decay photon lines (Fig. 4). Combined lifetime and gamma spectroscopy measurements allowed the unambiguous identification of all isotopes generated in the plethora of combinations of different nuclear reactions with the different materials present, see Fig. 6.

In all the samples, a striking feature is that the PET activity for the 511 keV lines is the dominant contribution to the radioactivity, as can be seen from Fig. 6 and also Fig. 5, which is just one example

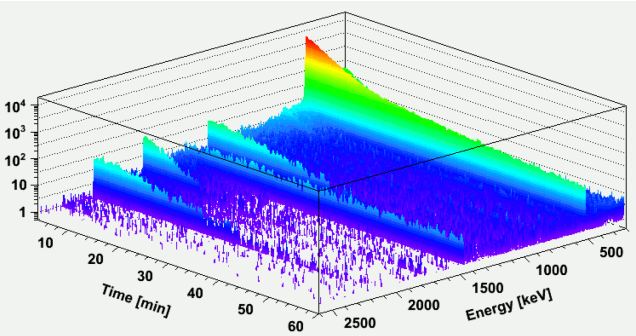

Fig. 4: Gamma spectroscopy in time differential mode allowing life-times for each gamma-line to be determined. This removes ambiguities in isotope identification. The 511 keV PET annihilation peak is the dominant feature.

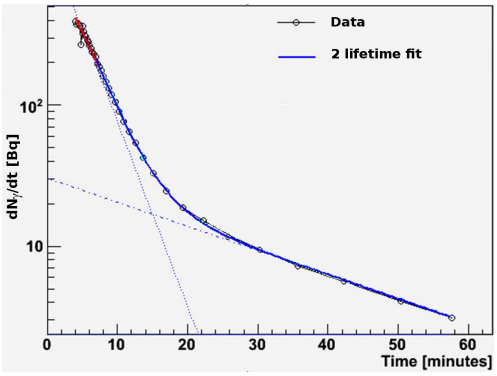

Fig. 5: Lifetime spectrum for the PET signal at 511 keV, isolated using the time coincidence condition. The short $\tau = 2$ min ^{15}O signal and the longer $\tau = 20$ min ^{11}C signal can be clearly seen.

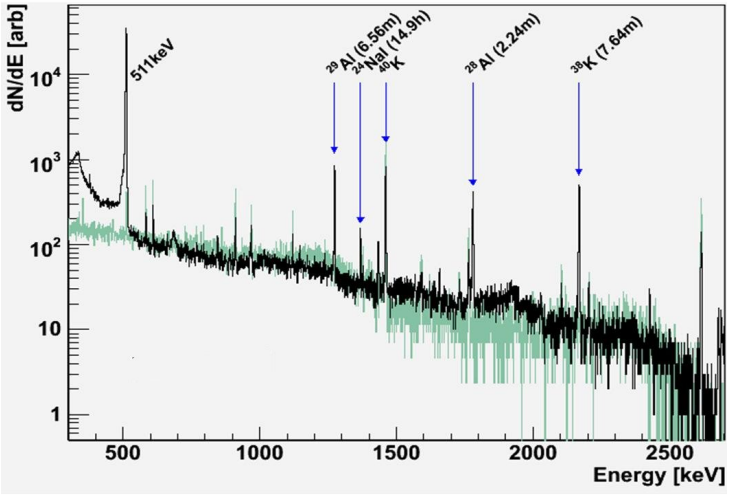

Fig. 6: Singles gamma spectroscopy results for kimberlite breccia taken 5 minutes after an irradiation dose of 50 Grays (the equivalent dose for the Mineral-PET system) where the accumulation time is 50 minutes. For comparison, a spectrum for non-irradiated or natural kimberlite is presented. The data acquisition is taken under the same conditions.

of extracting a lifetime for a particular gamma line. Initially this activity is dominated by the ^{15}O PET isotope (minutes after irradiation). The ^{15}O activity decays rapidly away (Fig. 5). After about 10 half lives (20 minutes), the ^{15}O is strongly suppressed (a factor of about 1/1000). At this stage, the dominant local concentration of PET activity would be the ^{11}C from a diamond, if it were present. Otherwise, there is expected to be a homogeneous background from both carbon- and oxygen- containing molecules. The remaining gamma lines are weak, and there is essentially an equivalent activity for the non-irradiated and the irradiated kimberlite spectrum. For example, the low level natural ^{40}K gamma line is easily visible in both spectra. Several other lines are identified, and labeled in the figure above, together with their lifetimes. In this data, the lifetimes are under an hour, except for a small amount of sodium, which has a lifetime of under a day. The Mineral-PET signal of ^{11}C (from a diamond) is clearly the dominant signal (per unit volume) in the spectrum (after a waiting period in the hold hopper).

Using the coincident detection facility, one could filter out the singles events (where there was no

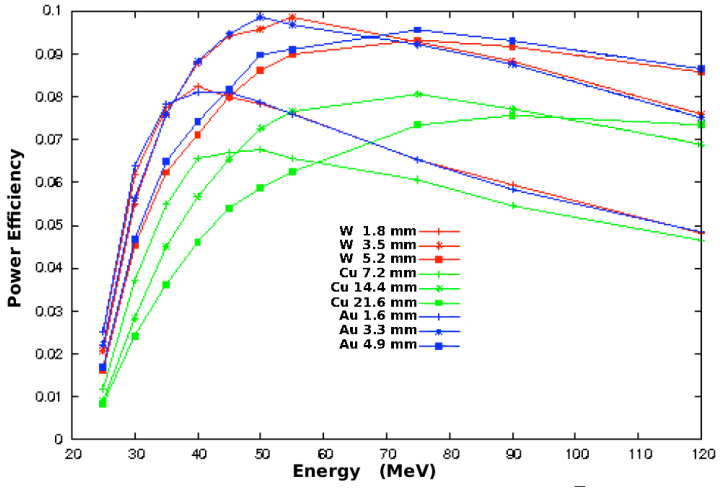

Fig. 7: A typical result from the GEANT Monte Carlo computer simulation of the performance of the high energy photon source. The curve levels out at 40 MeV, showing this is the lowest energy which can still efficiently produce photons in the range $E_\gamma = 20 - 27$ MeV. The power efficiency is defined in the text.

true coincidence in a 10 ns resolving time). The contribution to the PET activity could then be studied in greater detail, as has been seen in Fig. 5, where the $\tau = 2$ min and the $\tau = 20$ min lifetimes of ^{15}O and ^{11}C respectively are evident. The coincidences at the Mineral-PET counting time window are essentially only events where the 511 keV gamma photons are detected. At much longer times than in Fig. 5, a third component with about a 100 minute lifetime and a fourth component with about a 10 hour lifetime are evident. These have been identified as fluorine or titanium (created in nuclear reactions with oxygen or titanium) and copper (created in nuclear reactions with nickel). Irradiations up to a dose of 1.0 kGray were also carried out. This is 20 times the typical Mineral-PET dose. These samples were counted for 15 hours. The results matched those for the lower dose irradiations and indicated the Mineral-PET detector will be operating in very fine signal to noise conditions. Secondly, the issue of remnant activity for these samples is well understood and under good control. There does not appear to be any significant long lived ($\tau > 15$ hours) isotopic activity, and it is clear the kimberlite and the diamond are radiologically and environmentally safe within days of its irradiation.

In parallel to the experimental work, code was developed for first-order quantitative estimates of the production of collateral radioisotopes, from primary and secondary interactions with natural and prompt-decay isotopes, using published cross-section data and average energies from reaction kinematics. This code was used as a guide in the isotope identification during the data analysis. The results were consistent with the experiments.

2.3 Electron beam energy for the Activation process

The activation process for ^{12}C$(\gamma, n)^{11}$C using bremsstrahlung photons has been modeled with the Geant4 [15] Monte Carlo code to determine the optimal combination of electron beam energy, electron beam current and bremsstrahlung target thickness for conditions appropriate to Mineral-PET. A selection of these results are presented in Fig. 7. The quantity that has been optimized is the power efficiency, defined as the number of photons on-target, with an energy in the GDR region, per primary (beam) electron, normalized to the relative beam power, taken as $E_{e^-} = 40$ MeV. By simulating many different combinations of electron beam energy and current and bremsstrahlung target material and thickness, it was observed that the power efficiency tended to a plateau after about 40 MeV for the electron beam energy, for the most technically sensible choice of high-Z target, which was tungsten.

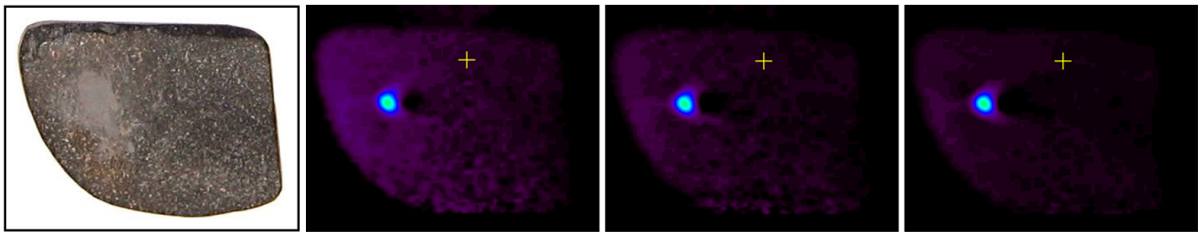

Fig. 8: A series of images of the density distribution of PET isotopes, taken at three consecutive 20 minute intervals starting at within 10 minutes after the irradiation. The homogeneous background decreases w.r.t. the diamond signal with delay time. The larger diamond is 0.5ct and the larger kimberlite sample about 5cm across.

2.4 Electron beam intensity for the Activation process

The identification of a diamond, implemented by the detection system discussed in later sections, requires a statistically significant signal above background. By combining the industrial requirements mentioned in the introduction with conservative estimates, both from analytical and Monte Carlo models of the efficiency of the complete detection system, we can estimate the source activity required, and from this the requirements for the irradiation process.

The decay rate of ^{11}C surviving at the time of detection from just the diamond is related to the electron flux as follows -

$$A(t) = \left[t_\gamma N_{^{12}\mathrm{C}} (e^{-x/X_0}) \left(\phi_{e^-} \frac{1}{\Delta E} \int_{\Delta E} P_{e^- \to \gamma}(E) \sigma_{(\gamma,n)}(E) dE \right) \right] \lambda_{^{11}\mathrm{C}} e^{-\lambda_{^{11}\mathrm{C}} t_h} \quad (1)$$

Here t_γ is the time of irradiation, $N_{^{12}\mathrm{C}}$ is the number of carbon nuclei in a diamond of given size, e^{-x/X_0} expresses the attenuation of the irradiation photons in the kimberlite host matrix, ϕ_{e^-} is the electron flux on the bremsstrahlung target, $P_{e^- \to \gamma}(E)$ and $\sigma_{(\gamma,n)}(E)$ are the probability and the cross section of the bremsstrahlung and (γ, n) processes respectively, E is the photon energy in the GDR region, ΔE is energy interval where this region is significant and $e^{-\lambda_{^{11}\mathrm{C}} t_h}$ accounts for the decay of the ^{11}C during the waiting time in the hold hopper.

With the knowledge of the kimberlite composition, the background activity from oxygen and sparse carbon can be estimated in the same way.

In the given scenario, with a throughput of kimberlite ore of 1000 tons per hour, resulting in a belt speed of 2 m/s and approximately 1 second for irradiation, and 1 second for detection, we calculate that it's necessary for the electron accelerator to deliver on the bremsstrahlung target a very high 5 mA average beam current (at an energy of 40 MeV as discussed above) in order to generate the flux of photons sufficient for the activation level required. Such an accelerator is achievable today.

2.5 Diamond within kimberlite by Medical-PET

A sample of kimberlite of mass 55 g was spiked with diamond of 0.5 carats. After an irradiation of 500 Grays, the kimberlite was transported to a small animal PET machine at the Karolinska Institutet where PET measurements were made. Figure 8 shows a photograph of the kimberlite samples, together with three sequential PET images. The PET images represent time integral acquisition for the three consecutive 20 minute intervals starting within 10 minutes of the irradiation. A slice has been made through the 3-D reconstruction at the position of the diamond, allowing the diamond to be clearly identified as a hotspot of PET activity. The ^{15}O signal becomes progressively less significant for later times. The dominant PET isotope in the last picture is from ^{11}C. The oxygen distribution is homogeneous, and the non-diamond carbon is also homogeneous but very dilute (about 0.2% atomic).

2.6 The effect of the activation process on diamond

The activation is performed over several layers of coarse crush kimberlite in the activation hopper. The radiation environment for the diamond particles within the kimberlite has several components. It firstly consists of the primary electron beam, which would have a distribution of energies up to the beam energy of 40 MeV, depending on the depth of the diamond within the kimberlite and the scattering history of the electron beam. The electrons would not penetrate significantly more than about halfway through the coarse crush kimberlite. Next there is the secondary photon beam, with a much lower flux than the electron beam, also with a distribution of energies (similar to the bremsstrahlung distribution). The penetration is still significant over about three layers of coarse crush rock for the highest energy of photon in the radiation hopper. Then, with once again a lower flux, suppressed by the cross section for these processes, would be the secondaries from nuclear reactions, including neutrons and light charged particles. These are not considered to be significant by comparison to the primary electron beam. The major interaction of the electron beam is via ionization. Bremsstrahlung photons must first produce a compton electron or a pair, and then once again the major interaction is via ionization. The Rutherfordian electron - carbon interaction is therefore relatively rare. Electrons are also kinematically disadvantaged in displacing carbon atoms, due to the high kinematic factor and the relatively large displacement threshold energy for diamond (25-80 eV and orientation dependent). The damage due to electrons has been measured in detail in the low MeV range, and modelled up to 10 MeV (see [16] and references therein). Extrapolating to the Mineral-PET conditions leads to a calculation that the vacancy related damage production would be less than an atomic fraction of 2×10^{11}. In the GeV range, studies are again available, see for example [17] and [18]. In this range the general result is that the electronic properties of ultra-pure synthetic diamond (which are very sensitive to damage) do not significantly deteriorate until a fluence of 10^{15} mips/cm^2. The Mineral-PET conditions are several orders of magnitude below this threshold. Natural diamond had its genesis typically 2 billion years ago. It endured a long residence time in the upper mantle in a context of the earths background radio-activity. It has also experienced violent geological processes at least during its eruption to the surface. The intrinsic defect concentrations are found to be orders of magnitude larger than the the expected damage due to the Mineral-PET technique. Natural diamond is also much too defected to be considered for electronic material. This reasoning is also confirmed by experiments which have not evidenced any detectable damage by optical spectroscopic techniques due to the Mineral-PET technique.

3 Detection

This section includes all the considerations which lead to the identification of a diamondiferous kimberlite rock. It is based on the PET technique, where the density of emissions from the PET isotope ^{11}C must be detected. The ^{A}X$(\gamma, n)^{A\text{-}1}$X reactions generates unstable, proton-rich nuclei which typically decay to a stable isotope by emitting a positron: $^{A\text{-}1}_{Z}\mathrm{X} \rightarrow ^{A\text{-}1}_{Z\text{-}1}\mathrm{Y} + e^{+} + \nu_e$. For the superallowed ^{11}C decay the pointlike Fermi theory is sufficient to provide information on the energy spectrum of the positron, which is of particular importance for this application, as it determines the distribution of the distance traveled by positrons before annihilation and consequently the smearing of the diamond signal [19]. In the case of the Mineral-PET detection of diamond, the endpoint of the beta spectrum for the decay $^{11}\mathrm{C}(\gamma, n)^{10}\mathrm{B}$ is at 0.96 MeV.

3.1 Spatial resolution

The emitted positron thermalizes mostly by the Bethe-Bloch mechanism in the host material. Its original emission direction is ultimately randomized by multiple scattering. The probability of in-flight annihilation is approximately inversely dependent on the velocity [20] and this process is therefore usually considered negligible (<2%) in favour of annihilation after thermalization. The decay positron thus travels some distance before it finally comes to rest (thermal energies) and annihilates with an electron from a neighbouring atom. The distribution of distances between the decaying PET isotopes and the point of an-

nihilation of the positron has been modelled for different PET isotopes in a water medium. It is generally a sharply peaked distribution with a substantial tail. In the case of ^{11}C in water, the FWHM and FHTM of this distribution is 0.188 mm and 1.86 mm respectively [21]. Scaling using the Bethe-Bloch formula from water to an average kimberlite yields range distributions for the decay positron of 0.063 mm and 0.63 mm for the FWHM and FWTM respectively. In non-metallic materials, the annihilation process can in first approximation be considered to proceed through a bound e^+e^- state, positronium (Ps), in the $S = 0$ or $S = 1$ states [22]. The energy difference between the two states is much less than thermal energies, so the relative population is typically (quantum) statistical, at 25% and 75% respectively. The annihilation of the $S = 0$ (para-positronium) state proceeds in the $e^+ + e^- \rightarrow \gamma\gamma$ channel, with a lifetime of about 100 ps, and the two 511 keV photons are emitted in opposite directions. The annihilation of the $S = 1$ state (orthopositronium) proceeds in the $e^+ + e^- \rightarrow \gamma\gamma\gamma$ channel, with a 3 orders of magnitude lower rate [23]. This results in a much longer lifetime, however the longer life makes it much more probable that "pick-off" interactions with host material electrons occur. The $S = 1$ state therefore also typically annihilates in the $\gamma\gamma$ channel [24], and once again we have the back-to-back two photon annihilation. The cases of in-flight annihilation and the residual momentum of positronium, or of the pick-up electron, can be effectively considered to cause a non co-linearity of the 2 gammas with a FWHM of 0.5 degrees [19] or 0.25 degrees [25]. For the geometry of mineral-PET, this is a smearing effect of 0.65 mm or 0.37 mm. Together with the range distribution of the positron, this effect also contributes to the lowest limit in imaging resolution. Finally, one may expect a physics limit to the resolution of imaging a PET source to be comfortably below 1 mm. It is therefore of interest to use a detection system with a resolution as close to this as possible.

3.2 The Technology Demonstrator

A scaled down planar PET array built around a conveyor delivery system (see Fig. 1) using kimberlite "phantoms" was constructed. As previously mentioned, the phantoms consisted of reconstituted kimberlite powder which had been homogeneously premixed with the positron emitter ^{22}Na. The reconstitution process used technology for radiation waste permanent storage, considering the background activity of the phantom. Diamonds were modeled in the phantom by the inclusion of a localized "hot-spot" of ^{22}Na. The activities of the homogeneous background as well as the localized PET emissions correlated with what was expected from kimberlite rock which had been subjected to the photon irradiation mentioned above. This detection environment is a worst case scenario, as one had the $E_\gamma = 1274$ keV decay photon of ^{20}Ne in close coincidence with the annihilation photons. This is a background that will not be present in the real Mineral-PET system. In this Technology Demonstrator, phantom activities, arrangements, delivery speed and diamond simulant activity can be varied, as well as parameters and configurations of the detection system. The mechanical setup was designed in collaboration with the industry partner of the project, taking into account both the mechanical and industrial requirement, and the physics requirements, in particular gamma absorption and radiation damage characteristics of the materials.

3.2.1 PET detectors

There are currently several options for the detection of the 511 keV gamma rays from e^+e^- annihilation in PET imaging systems. In the planar PET array of the technology demonstrator, we have used inorganic scintillators and photomultiplier tubes (PMT). This choice was predicated by simplicity, affordability and flexibility for testing various apparatus configurations. Scintillators detect the passage of ionizing radiation by emitting photons inside or near the visible band, which can then cause the emission of electrons from the photosensitive cathode of the PMT. In order to design an effective detector, capable of providing not just energy and timing information, it is necessary to adequately consider the coupled problems of the scintillation emission spectrum, photocathode characteristic spectral sensitivity; optical characteristics of the scintillator, PMT glass and coupling material; optical reflection, refraction and diffusion from the different interfaces. This is especially true when dealing with the stringent requirements for position

sensitivity, combined with a scintillator with low light-output like BGO. It is also necessary to consider the different processes by which the gamma photon, a neutral particle, deposits energy in the scintillator. At this energy well below the pair production threshold, the most significant interactions are the photo-electric effect [26, 27], Compton scattering, Rayleigh scattering and photonuclear absorption. The low energy of these interactions causes them to depend on the detailed electronic structure of the target material, such that for accurate simulation it is necessary to resort to semi-empirical or data-driven models based on experimental measurements [28]; but already an elementary treatment can provide indications on the different Z dependence of these processes, useful for the choice of scintillation material [29].

Inorganic crystal scintillators have since long demonstrated their excellent qualities for detection of gamma rays in the 100 keV-500MeV range. While NaI(Tl) (thallium-doped sodium iodide) is still the golden standard in this class of detectors, BGO (bismuth germanate - $Bi_4Ge_3O_{12}$) and, more recently, LSO (lutetium orthosilicate) have been the preferred choice for use in medical PET machines, where the lower energy resolution is less important, and the shorter radiation length decreases the inconveniences of the parallax effect [30]. Our research has indicated that BGO is currently the optimal compromise between desirable properties and cost. The readout of optical photons from the scintillating crystal is achieved with a multi-wire anode Position Sensitive Photomultiplier Tubes (PS-PMT [31]), which allows for high position resolution with a limited number of readout channels (compared to multi-pad PS-PMTs) and without the need of specially designed crystals (needed for the multi-PMT approach most commonly used in medical PET). The whole detector has been the subject of very detailed Monte Carlo simulations, including positron straggling and annihilation, gamma scattering and absorption in the host rock, energy deposit in the scintillator material, and production and propagation of the optical photons from scintillation to the PS-PMT photocathode, considering the specific optical properties of materials and surfaces. While a comprehensive implementation has been realized within the Geant4 toolkit [32], we also obtained useful guidance and insight from a much simplified simulation of the optical system, developed independently. These simulations have been confirmed by the experimental results, and have been fundamental in optimizing the planar PET array design and in scaling calculations.

3.2.2 Signal processing, trigger and DAQ

The readout electronics chain has a total of 64 fully independent and tunable channels (4 channels for each of the 16 PS-PMTs), with amplitude and time readout on each one separately, plus a simple but flexible trigger system. Each of the four outputs of each PS-PMT is first processed by an ad-hoc shaping preamplifier (8-channel units by ASCOM on design of Prof. Bassini - INFN Milan); the resulting signal is then fed to a dual amplifier that provides both a slow (1-3 μs) shaped spectroscopy output, and a fast differential output (16-channel CAEN N568B). The shaped output is connected directly to the signal inputs of the 32-channel peak ADCs, while the fast output goes to the 16-channel Constant-Fraction Discriminators (CAEN N483) The hardware logic that triggers the readout of an event implements the basic requirement of a chosen number of channels being above a certain threshold, with few requirements on their spatial location. This is presently considered sufficient for the Technology Demonstrator, where the rates are relatively low. The final detector will require a more sophisticated trigger to fully exploit the space-localized time coincidence of back-to-back gammas, and reduce the readout rate to acceptable levels. The digital readout comprises the mentioned peak ADCs (CAEN V792) and a 64-channel, free-running clock-based TDC (CAEN V1190); these are VME based units, controlled by a VME single board Intel-based controller running Scientific Linux 4 and, for maximum flexibility and performance, an ad-hoc DAQ software based on low-level libraries adapted from the Open Source MIDAS [33] DAQ software.

3.2.3 Medical-PET imaging

In common medical PET a few different classes of algorithms are used to reconstruct a 2 or 3 dimensional image of the subject. The original and conceptually simpler method is the Filtered Back-Projection

(FBP) method, in which a modified inverse Radon transform, applied to 1-dimensional projections of a 2-dimensional object, is used to infer the shape of the object; the process is repeated for multiple 2D "slices" of the object (from which originated the name *tomography*). In order to reduce noise artifacts, different types of filters are used with the basic FBP. Modifications of the FBP, which take advantage of more modern "3D" PET detectors (without gamma absorbing tungsten septa), are commonly used for so called $2\frac{1}{2}$D or 3D imaging. The Iterative Reconstruction methods instead assume an initial source distribution, forward-project it into sinograms and compare these with the actual data to correct the distribution, iterating until convergence; they are not yet commonly used for human PET, because they are more computationally intensive than FBP. On the other side, IR methods do not suffer as much from noise and from incompleteness of the set of projections. For a review of PET imaging, see e.g. [34]. In general, both FBP and IR methods are reliant on high statistics data sets, and especially the FBP methods need a detector which covers nearly a 2π planar angle around the subject. Both of these conditions are in conflict with the requirements in Mineral-PET, because the transport of the samples imposes a planar or nearly planar geometry, and the limits on the attainable activation of the rocks severely constrain the statistics that will be collected for each sample.

3.2.4 Mineral-PET Fast Quasi-imaging and Identification algorithm

A completely different approach to imaging is necessary in Mineral PET (lower statistics, shorter processing times). The first Mineral-PET quantitative imaging method is a "tubes and voxels" method. Each time a colinear coincident pair of annihilation photons is detected, the endpoints of a line which intersect each plane of the planar PET array are registered. This line may be thought of as a tube, once the effect of position resolution has been considered. Each PET event therefore generates such a tube in the memory of the acquisition system. Instead of accumulating the event-by-event statistics in sinograms, the back-projection concept is applied independently for each event, in an approach that is more similar to what is done in High Energy Physics analysis for track reconstruction; the statistics of the crossing of tubes with specific volume elements (voxels) are then accumulated in a 3D lattice of voxels, with a pitch similar to the position resolution of the detector. This approach would be too computationally intensive in the high statistics case of the medical applications, but it is feasible in the Mineral-PET case, and it has the advantage of conserving the full information content of the limited number of detector hits. The quantitative identification of a hot spot of positron emission, corresponding to the high concentration of ^{11}C in a diamond, can then be based on the statistical information contained in the voxel lattice. The most straightforward method is to search the whole lattice for voxels with higher statistics, above the statistical fluctuations of the background. This simple method already produces acceptable results for all but the smallest diamonds, and has the advantage of being amenable to an analytic study of the identification efficiency. Already for this simplest method, it is necessary to implement a non-trivial search algorithm on the very large 3D lattice of voxels, to reduce the data processing time to acceptable levels. This identification algorithm has been studied on simulated data from a simple Monte Carlo event generator, with focus on the performance in terms of efficiency and false signal rejection as a function of various parameters - primarily the signal and background activity levels.

A critical advantage of this approach to imaging and identification, over more traditional PET techniques, is its being amenable to an aggressive parallelization of the computation, which guarantees an easy and cost-effective scalability to large detection arrays.

In the case of the Technology Demonstrator, the phantoms are moving on the conveyor belt as they progress through the planar PET array. The data from the acquisition system presents a n-tuple where each event in the n-tuple contains the the energy and position (E, x, y, z) at the PET detector as recorded for each photon of the coincident pair, within a resolving time of 20 ns. A time stamp for the event accurate to milliseconds is also recorded with the event. Using the belt speed, the events can be mapped back spatially to remove the effect of the belt motion. The Mineral-PET algorithm of incrementing the 3-D histogram of voxels for each tube crossing can then be implemented. The right

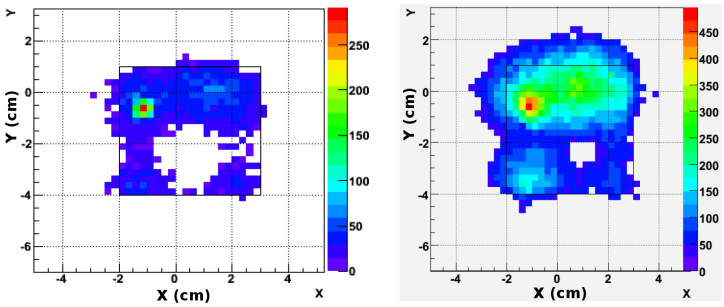

Fig. 9: good match with MC simulations.

hand part of Fig. 9 represents a slice through the 3-D histogram for an acquisition time corresponding to a single pass through of the moving kimberlite phantom, after the motion correction. The slice is at the position of the diamond simulant activity. Even at these low statistics, the diamond simulant is clearly recognizable even before further processing by the Mineral-PET algorithm, which is effectively a search for significant correlated deviations from the background activity followed by a peak characterization in 3-D.

3.2.5 Full Monte Carlo simulation

The entire planar PET array has been modelled with Monte Carlo techniques, to describe the phantom activity, the full geometry of the system, the materials involved and the active detector components. The output from the Monte Carlo simulation is formatted in the same structure as real data, and the simulated data can be processed by the analysis engine identically to the real data. The left hand part of Fig. 9 represents a model of the same experiment described above for a given phantom passing through the Technology Demonstrator. The model has the simulant diamond activity in a similar place to the real phantom, and the same slice through the 3-D histogram is presented. The Monte Carlo simulation agrees with the real experiment extremely well. The apparent "holes" in the background activity are also well modelled. These relate to issue of regions between the detectors which are not active, so that there is not full coverage in this implementation of the planar PET array. This leads to a variation in the coincident detection efficiency which has not been normalized out in this figure. It demonstrates the excellent correspondence between the simulation and the experiment, and evidences the system is well understood. The understanding of the system, as confirmed by the Monte Carlo simulation, has been used in the scaling of the results from the technology Demonstrator to a possible future full scale implementation of the the Mineral-PET.

4 Conclusion

Mineral-PET has been described as an ore-sorting technique to identify diamondiferous kimberlite in an online mining context. It is based on Medical-PET, but with modifications to allow operation at higher throughput taking advantage of several features: the favourable strong and easily discriminated co-incident ^{11}C PET signal compared to even the singles radiation, enormous contrast in the diamond PET signal over the background and the fact that a statistical decision can be made without implementation of conventional PET imaging.

The results of tests with the technology demonstrator coupled with extensive Monte Carlo modelling have confirmed the minimum activity of ^{11}C necessary in order to identify a minimal size diamond (1 mm diameter) at a given confidence level. This information can be scaled for the full Mineral-PET detector, leading via equation (1) as well as a Monte Carlo simulation to minimal requirements for the specifications of the electron accelerator. The specifications are demanding ($E_e = 40$ MeV at 5 mA and quasi-continuous time structure), but feasible. This enables Mineral-PET to conceivably be deployed up

to run-of-mine conditions (100-1000 tons of rock processed per hour). It is expected that this technology will reduce the costs of the recovery process. There will be much less processing of the mine rock. Only a coarse pre-crush is necessary. The barren rock is not subjected to further processing. In addition, this technology will improve the yield of large diamonds. One may also implement a differentiated extraction process. It becomes viable to implement more sophisticated recovery techniques. The total yield of the mine is also expected to improve. The saving in costs and energy also impact on the viability and sustainability of the mining programme and dramatically allieviate the environmental impact.

Acknowledgements

Funding from the National Research Foundation of South Africa in the THRIP program in conjunction with Bateman Engineering is acknowledged. The valuable help of the following colleagues is acknowledged : J Chapman (Rio Tinto, Australia), R Bassini (INFN and Physics Dept. Milano University), P Aggerholm and S Pape-Møller (Physics Dept. Århus University), R Ruth and J Rifkin (Lyncean Technologies, Inc, California), S-L Wong (L-3 Services, Inc.), B Lindt and A Brahme (MRP, Karolinska Institutet and C-RAD AB, Sweden). The involvement of the iThemba LABS (Gauteng) in Johannesburg is acknowledged for hosting the Technology Demonstrator and for technical support.

References

[1] M. S. H.O.A. Meyer, *Natural Diamond, Ch. 10 in Handbook of industrial diamonds and diamond films* (CRC Press, 1988).

[2] J. Sellschop and S. Connell, *SA Patent : Detection of Diamond* (ZA 2004/2010, 2006/08025).

[3] G. Muehllehner and J. Karp, Phys. Med. Biol. **51**, R117 (2006).

[4] G. C. Baldwin and G. S. Klaiber, Physical Review **711**, 3 (1947).

[5] M. Goldhaber and E. Teller, Physical Review **74**, 1046 (1948).

[6] S. DeBenedetti, *Nuclear Interactions* (London: JohnWiley & Sons, 2 ed., 1967).

[7] J. Eisenberg and W. Greiner, *Nuclear Models - Collective and single particle phenomena, vol. 1 of Nuclear Theory* (, 1970). Amsterdam: North-Holland Publishing Co., 1 ed.

[8] J. Speth and A. van der Woude, Reports on Progress in Physics **44/7**, 719 (1981).

[9] F. Lewis, J. Walecka, J. Goldemberg, and W. Barber, Physcal Review Letters **10**, 493 (1963).

[10] F. Malik and M. Mustafa, *Proceedings of the Fifth symposium on the structure of low-medium mass nucleiifth symposium on the structure of low-medium mass nuclei* (J.P. Davidson and B.D. Kern, eds.), , Univ. Kentucky, 1973).

[11] A. Fassò, A. Ferrari, and P. Sala, *Total giant resonance photonuclear cross sections for light nuclei: a database for the FLUKA Monte Carlo transport code, in Shielding Aspects of Accelerators, Targets and Irradiation Facilities (SATIF 3)* (OECD-NEA, 1998).

[12] M. White, R. Little, and M. Chadwick, *Proceedings of the ANS on Nuclear Applications of Accelerator Technology, (Long Beach, California) November 14-18* (, 1999).

[13] M. Chadwick, *Handbook on photonuclear data for applications: Cross sections and spectra, Tech. Rep. IAEA-TECDOC-1178* (IAEA, Vienna, 2000).

[14] F. Gallmeier, Radiation Protection Dosimetry **116/1-4**, 264 (2005).

[15] S. Agostinelli *et al.*, Nuclear Instruments and Methods in Physics Research A **506**, 250 (2003).

[16] B. Campbell and A. Mainwood, Phys. Stat. Sol.(a) **181**, 99 (2000).

[17] W. Adam *et al.*, Nuclear Instruments and Methods in Physics Research A **511**, 124Ű131 (2003).

[18] J. Isberg *et al.*, Science **297**, 1670 (2002).

[19] S. Derenzo, *Positron Annihilation (R. R. Hasiguti and K. Fujiwara, eds.)* (Japan: Sendai, 1979).

[20] P. Dirac, Proc. Cambridge Philos. Soc. **26**, 361 (1930).

[21] C. Levin and E. Hoffman, Physics in Medicine and Biology **44/3**, 781 (1999).

[22] A. Igarashi, I. S. M. Kimura, and N. Toshima, Physical Review A **68**, 042716 (2003).

[23] A. Czarnecki, Acta Phys. Polon. **B30**, 837 (1999).

[24] R. Krause-Rehberg and H. Leipner, *Positron Annihilation in Semiconductors: Defect Studies* (Springer Series in Solid-State Sciences, 2003).

[25] S. Chetty, J. Sorenson, and M. Pghelps, *Physics in Nuclear Medicine* (WB Saunders, New York, 2003).

[26] L. Mairie, *Photoelectric effect - Geant4 Tutorial at SLAC, February* (, 2002).

[27] F. Biggs and R. Lighthill, *Analytical approximations for X-ray cross sections III," Tech. Rep. SAND-87-0070* (SANDIA, 1988).

[28] D. Wright *et al.*, *Geant4 - Physics Reference Manual," Tech. Rep.* (Geant4 Collaboration, 2006).

[29] S. Derenzo, W. Moses, R. Huesman, and T. Budinger, *Critical instrumentation issues for <2 mm resolution, high sensitivity brain PET* (Amsterdam: Elsevier Science Publishers, 1993).

[30] G. Blasse, Chem. Mater. **6**, 1465 (1994).

[31] *Hamamatsu Photonics KK, "Hamamatsu R2486 Position-Sensitive Photomultiplier Tubes with crossed wire anodes." Specifications and Information Sheet* (, 2001).

[32] S. Agostinelli *et al.*, Nuclear Instruments and Methods A **506-3**, 250 (2003).

[33] *PSI and TRIUMF laboratories, "The MIDAS DAQ system."* , `http://midas.psi.ch/`.

[34] D. Townsend, Molecular Imaging and Biology **6/5**, 275 (2004).